A Practical Approach for Targeting Structural Variants Genome-wide in Plasma Cell-free DNA

Michael M. Murata[1¶], Fumie Igari[1,2¶], Ryan Urbanowicz[3], Lila Mouakkad[1], Sungjin Kim[4], Zijing Chen[4,5], Dolores DiVizio[1,4], Edwin M. Posadas[4,5], Armando E. Giuliano[1,4], and Hisashi Tanaka[1,4,6,*]

[1]Department of Surgery, Cedars-Sinai Medical Center, West Hollywood, CA 90048, USA

[2]Department of Breast Oncology, Juntendo University, Tokyo, Japan

[3]Department of Computational Biomedicine, Cedars-Sinai Medical Center, West Hollywood, CA 90048, USA

[4]Cedars-Sinai Cancer, Cedars-Sinai Medical Center, West Hollywood, CA 90048, USA

[5]Department of Medicine, Cedars-Sinai Medical Center, West Hollywood, CA 90048, USA

[6]Department of Biomedical Sciences, Cedars-Sinai Medical Center, West Hollywood, CA 90048, USA

[*]Corresponding author: Hisashi Tanaka (hisashi.tanaka@cshs.org).

¶These authors contributed equally to this work.

Plasma cell-free DNA (cfDNA) is a promising source of gene mutations for cancer detection by liquid biopsy. However, no current tests interrogate chromosomal structural variants (SVs) genome-wide. Here, we report a simple molecular and sequencing workflow called Genome-wide Analysis of Palindrome Formation (GAPF-seq) to probe DNA palindromes, a type of SV that often demarcates gene amplification. With low-throughput next-generation sequencing and automated machine learning, tumor DNA showed skewed chromosomal distributions of high-coverage 1-kb bins (HCBs), which differentiated 39 breast tumors from matched normal DNA with an average Area Under the Curve (AUC) of 0.9819. A proof-of-concept liquid biopsy study using cfDNA from prostate cancer patients and healthy individuals yielded an average AUC of 0.965. HCBs on the X chromosome emerged as a determinant feature and were associated with androgen receptor gene amplification. As a novel agnostic liquid biopsy approach, GAPF-seq could fill the technological gap offering unique cancer-specific SV profiles.

Introduction

Genome instability stands out as a defining hallmark of cancer.[1-5] Changes at the single nucleotide level (i.e., mutations) can activate oncogenes or inactivate tumor suppressor genes. Equally prevalent are structural rearrangements of large chromosomal segments, referred to as structural variants (SVs), such as duplications, deletions, and translocations. These genetic changes are the primary drivers of malignant transformation, disease progression, and therapy resistance. Beyond these roles in cancer biology, tumor-specific DNA changes can serve as biomarkers for cancer detection, which has gained momentum in the context of liquid biopsy.[6,7] Liquid biopsy holds promise as less invasive and more repeatable assessments compared to currently available methods at the clinic such as needle biopsies or imaging scans. Traditionally, blood has been a source of protein biomarkers such as prostate-specific antigen (PSA).[8] More recently, with the advent of DNA-analyses technologies for cancer genomes, DNA released into the blood from tumor cells, termed circulating tumor DNA (ctDNA) has become a mainstream target for developing liquid biopsy-based clinical tests. Several Food and Drug Administration (FDA) approved tests are currently in clinical use.[9-14] These tests identify tumor-specific mutations in cell-free DNA (cfDNA) isolated from plasma, either by a single-gene platform or by Next-Generation Sequencing (NGS) for multiple cancer genes (i.e., targeted sequencing). While reporting residual tumor burden and actionable mutations for advanced cancer patients, there is a potential for extending mutation detection in plasma cfDNA to cancer screening in the general population. However, even non-malignant hematopoietic cells accumulate clonal mutations in cancer-associated genes such as *p53* and *KRAS*.[15-17] This phenomenon termed clonal hematopoiesis complicates the use of mutations as effective cancer-specific agnostic biomarkers. Additionally, because ctDNA represents only a small fraction of the total cfDNA, particularly in patients with early-stage tumors (referred to tumor fraction, TF),[18] ctDNA detection requires high sensitivity.

Alternatively, SVs are plausible cancer biomarkers. Nevertheless, SVs have not been pursued for liquid biopsy targets as rigorously as mutations and other emerging targets based on epigenetic features, such as DNA methylation and cfDNA fragmentation patterns. SVs often present as DNA copy number alterations (CNA), but the detection of CNA also suffers from very low TF.[19,20] Tumor-specific translocations can be detected by discordant mate pairs in whole genome sequencing (WGS) data.[21] However, the detection of SVs

by mate-pair analyses requires deep coverage and can be computationally challenging when applied to cfDNA with low TF. *In silico* selection of naïve short DNA fragments (<150 bp) for WGS libraries could enhance CNA signal in cfDNA.[22] However, our knowledge on ctDNA fragment sizes and the utility in enhancing tumor detection may evolve over time, as other studies reported that cfDNA fragment sizes in cancer patients' plasma exhibits greater variability (both longer and shorter) compared to the fragment sizes of healthy individuals' cfDNA[23,24]. Additionally, tumor-derived high molecular weight DNA in cancer patients' plasma has also been documented.[25]

The challenges of low TF in cfDNA can be addressed by enriching cancer DNA-specific features through *in vitro* cfDNA processing. To explore this novel concept, we employed our SV-targeting technology known as Genome-wide Analysis of Palindrome Formation (GAPF).[26-30] The targeted SVs in this case are DNA palindromes, also referred to as inverted repeats or fold-back inversions,[31] defined by DNA sequences identical to their reverse complements (Fig. 1A). While large (>10 kb) germline palindromes are characteristic of sex chromosomes,[32,33] DNA palindromes in cancer emerge *de novo* through the inverted duplication of single-copy DNA sequences.[26] Multiple palindromes can form during Breakage-Fusion-Bridge (BFB) cycles. BFB cycles are initiated by a chromosome with two centromeres, called dicentric chromosomes. BFB cycles are major drivers of genome instability and genomic amplification, as dicentric chromosomes arise from common processes in genome instability such as illegitimate repair of DNA double-strand breaks (DSBs), fusions of dysfunctional and critically short telomeres, and translocation gaining two centromere-bearing chromosomes.[34-36] Notably, anaphase bridges, an indication of segregating dicentric chromosomes, were observed in preneoplastic regions.[37] Therefore, DNA palindromes can arise very early during carcinogenesis and may serve as valuable cancer biomarkers throughout cancer development and progression. We have previously shown that DNA palindromes can be enriched *in vitro* from genomic DNA using a straightforward molecular procedure. Importantly, we have demonstrated palindrome detection in cancer DNA even in 25-fold excess of normal DNA,[26] which underscores the potential of GAPF for cancer detection in samples with low tumor DNA fraction, such as plasma cfDNA. In this study, we applied the principles of GAPF to plasma cfDNA for the first time, developing new procedures optimized for small amounts of cfDNA. We also introduced an NGS and bioinformatics analysis pipeline for the development of cfGAPF-seq for plasma cfDNA. By employing machine learning algorithms for binary classification in the analytical pipeline, we assessed the capability of

cfGAPF-seq to detect cancer DNA in plasma cfDNA, presenting a new tool for liquid biopsy. Our findings indicate that cfGAPF-seq can differentiate cancer patients' plasma cfDNA from normal DNA and healthy individuals' plasma cfDNA, even in cases of low TF. These results highlight the potential of cancer-specific SVs as sensitive biomarkers in liquid biopsy.

Results

Palindrome Detection by GAPF-seq

A new protocol for the Genome-wide Analysis of Palindrome Formation (GAPF) was adapted to contend with the low amounts of cell-free DNA (cfDNA) in plasma (**Fig. 1A**). In brief, input genomic DNA (as low as 30 ng) underwent initial digestion with relatively infrequent cutting enzymes. Subsequently, the DNA was boiled for denaturation and promptly quenched in ice water to facilitate the rapid self-annealing of palindromic sequences (i.e., snap-back).[26,38] The resulting DNA was then subject to digestion using the single-strand specific nuclease S1. The junctions of palindromic DNA could self-anneal following denaturing by boiling, re-forming double-stranded DNA (dsDNA) and becoming resistant to S1. In contrast, non-palindromic sequences would be digested by S1 after denaturation. The remaining dsDNA was ligated with sequencing adaptors and amplified during library construction. Resulting sequencing libraries would be enriched with palindromic junctions.

The sequencing reads from GAPF-processed DNA were aligned to the hg38 human reference genome and quantified in 1 kb non-overlapping bins (**Fig. 1A**). An accumulation of reads in these 1 kb bins would lead to high coverage, and consequently, high coverage bins (HCBs) may indicate the presence of DNA palindromes.[28,39] Indeed, when genomic DNA of Colo320DM cell line was processed by GAPF and sequenced, HCBs were seen in known palindromic junctions on chr1 at *RPRD2*, *ECM1*, and *CTSK* (**Fig. 1B**).[28] To simulate a low tumor fraction (TF), as expected from plasma cfDNA, Colo320DM DNA was *in vitro* diluted with IMR90 normal fibroblast DNA *in vitro* prior to GAPF. HCBs were consistently detected at *RPRD2*, *ECM1*, and *CTSK* for all dilutions. No such peaks were apparent in the corresponding region of GAPF-seq data from IMR90 DNA (**Fig. 1B**, 100% IMR90). The average normalized read coverage (number of sequencing reads per bin divided by a per-million scaling factor) for HCBs at *CTSK* was 65.5 for 100% Colo320 input DNA and decreased exponentially by dilution (**Fig. 1C**). This exponential trend was similarly observed for *RPRD2* and *ECM1*. The

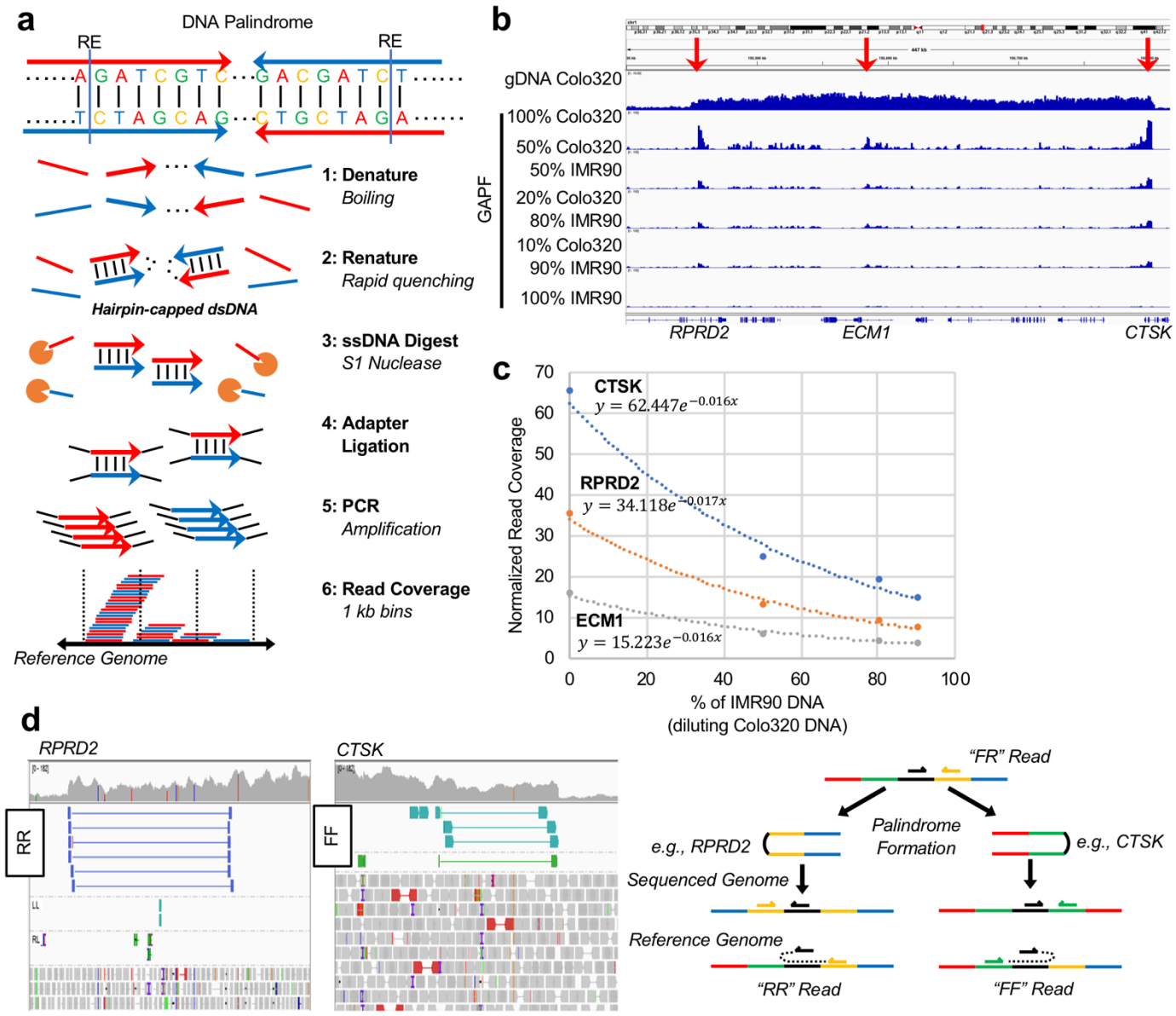

Fig. 1: Genome-wide Analysis of Palindrome Formation (GAPF) enriches structural variants.
a DNA palindromes are genomic regions with sequences that are reverse compliments of each other and could span large genomic segments. Genomic DNA was first digested with restriction enzymes (RE), by which only palindromic junctions folded-back to hairpin-capped dsDNA after denaturing DNA by boiling and rapidly renaturing in an ice water quench. Non-palindromic DNA, including DNA liberated from palindromic junctions by RE, was digested by S1 nuclease. Note that S1 also digested the hairpin part of DNA from palindromic junctions. Following adapter ligation to dsDNA and amplification by PCR was done as a part of NGS library construction. Read coverage was quantified in 1 kb bins genome-wide. **b** Read coverage in 1 kb bins for genomic or GAPF DNA is visualized using the Integrative Genomics Viewer (IGV). Colo320 colorectal adenocarcinoma cancer cell line DNA is diluted by IMR90 normal fibroblast DNA prior to GAPF. Peaks in GAPF data are observed at known palindromic junctions on chr1, including *RPRD2*, *ECM1*, and *CTSK*. **c** The GAPF read coverage decreases following an exponential trend at *RPRD2* (R2 = 0.9908), *ECM1* (R2 = 0.9848), and *CTSK* (R2 = 0.9776) as the amount of diluting IMR90 normal DNA increases. **d** Paired sequencing reads can have anomalous orientations such as "reverse-reverse" (RR) or "forward-forward" (FF) at sites of structural rearrangements near known palindromic junctions in Colo320 cancer cell line DNA (left). A schematic illustrating how palindromes generate RR or FF read pairs is presented (right).

lowest peak was detected at *ECM1* in 10% Colo DNA with an average read coverage of 3.67. Since the average read coverage genome-wide was approximately 0.31, GAPF-seq remains capable of reliably detecting palindromic signals after 10-fold dilution.

Paired-end sequencing offers the advantage of utilizing the relative orientation of mate pairs to confirm the presence of palindromes within amplified genomic segments. In WGS data, mates facing in the same direction (e.g., forward-forward, FF, and reverse-reverse, RR) concerning the reference genome can be identified at the ends of the amplified region within 1q21. FF or RR read pairs were identified in publicly available deep coverage WGS data (**Fig. 1D**)[40], but not our shallow WGS, possibly due to the underrepresentation of secondary structure-forming DNA in sequencing libraries. Navigating the secondary structure of palindromic DNA during PCR, which is an integral part of library construction processes, is widely known to be a challenging task.[41,42]

GAPF-seq for Breast Tumor DNA

To evaluate the ability of GAPF-seq to differentially call tumor DNA from normal DNA, we collected tumor and normal GAPF-seq data from 39 pairs of fresh frozen breast tumors and matched leukocytes (buffy coat) (**Supp Table 1**). These breast tumors included both triple-negative breast cancer (TNBC) and luminal breast cancer subtypes, with stages ranging from Stage I to Stage IV (**Fig. 2A**). Following GAPF processing, sequencing reads were counted in 1 kb bins genome-wide and the read coverage was calculated as outlined above (**Fig. 1A**). To test the reproducibility of GAPF-seq, we assessed the average read coverage in each cytoband (instead of 1 kb bins) throughout the genome using GAPF-seq replicates from seven pairs of tumor and normal DNA (**Fig. 2B, Supp Fig. 1**). The read coverage at the cytoband level showed remarkable consistency, with an intraclass correlation coefficient of 0.9971 (95% CI: 0.9966-0.9974), confirming the reproducibility of the assay.

A vast majority of 1 kb bins (approximately 3,130,000 bins out of 3,209,513 total bins) in both breast tumor and buffy coat DNA exhibited an average read coverage less than 5, likely attributed to the digestion of non-palindromic sequences by S1 nuclease. However, there was a notable difference in the 1 kb bins with read coverage > 5 between tumor and normal samples (**Fig. 2C**). Particularly at higher coverage ranges (read coverage > 10), tumor GAPF-seq data displayed a greater number of bins than normal GAPF-seq data, indicting the potential presence of tumor-specific palindromes. This observation formed the basis for delineating HCBs as means to differentiate tumor and normal DNA.

a

Subtype /pStage	I	II A	II B	III A	III C	IV	N/A	Count
Lum	4	14	7	3	1	1	2	32
TNBC	3	2	1	0	1	0	0	7
Total	7	16	8	3	2	1	2	39

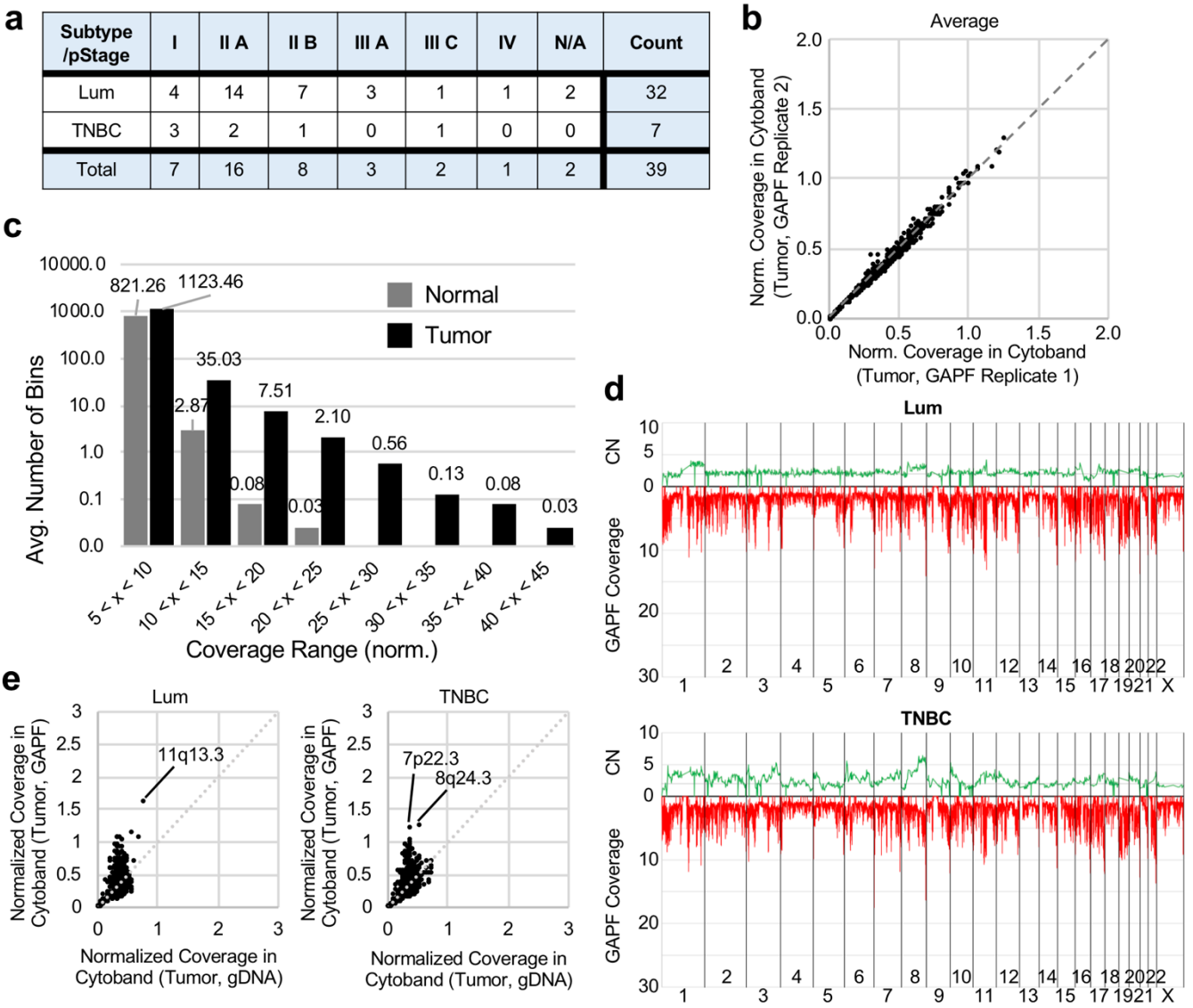

Fig. 2: High coverage 1 kb GAPF bins are tumor-specific.
a A table showing the breast cancer subtype and pathologic stage (pStage) for 39 breast tumors used for GAPF. **b** The GAPF read coverage in cytobands is normalized by the size of the cytoband (in bp) and averaged for the seven (7) duplicates. The normalized read coverage in each cytoband for the first set of replicates is plotted against the duplicates with an intraclass correlation coefficient of 0.9971 (95% CI: 0.9966-0.9974). **c** The average number of 1 kb bins with normalized read coverages in different ranges from 39 breast tumors and matched normal. Out of the 3,209,513 bins in the human genome, the majority exhibit very low read coverage in the range between 0 and 5 (not shown). At higher coverage ranges, the average number of bins with high coverage is greater in tumor compared to normal. **d** The average copy number (CN) is plotted against the average GAPF read coverage for luminal (Lum) breast tumors (top, n = 26) and triple negative breast cancer (TNBC) tumors (bottom, n = 5). **e** The GAPF read coverage in cytobands is normalized by the size of the cytoband (in bp). The normalized read coverage in each cytoband for genomic DNA (gDNA) is plotted against GAPF DNA and averaged for Lum (left, n = 26) or TNBC (right, n = 5) tumors.

As DNA palindromes are frequently associated with genomic amplification, the average copy number (CN) of chromosomal segments from shallow WGS data was plotted against the read coverage of GAPF-seq data for 26 luminal and 5 TNBC tumors (**Fig. 2D**). Overall, TNBC showed more CNA than luminal breast tumors, aligning with previous reports.[43] While genome-wide GAPF read coverage appeared indistinguishable between subtypes, a closer look at GAPF-seq and WGS data from individual pairs revealed unique subtype

coverage patterns. For example, patient 14-990 with TNBC exhibited significant genome-wide CNA (**Supp Fig. 2A**), and GAPF-seq revealed a notable read enrichment in cytoband 8q24.3 that correlated to increased CN. In contrast, a patient with luminal breast cancer (14-752) showed CNA and increased GAPF coverage localized primarily to cytoband 11q13 (**Supp Fig. 2B**). The coverage from GAPF-seq data was plotted against that from WGS at the cytoband level (**Fig. 2E**). Overall, cytobands 11q13.2-5 were enriched in luminal tumors, while cytoband 8q24.3 was predominant in TNBC.

Tumor DNA Calling Algorithm by GAPF-seq

Upon further inspection of regions of high GAPF coverage, we observed common enrichment in several bins across both tumor and normal samples (**Supp Fig. 3**). We explored the possibility of germline palindromes.[44,45] Alternatively, we considered that specific DNA segments were resistant to denaturation, and consequently, these segments would be resistant to S1 nuclease, leading to amplification during library construction. GC-rich regions of DNA are not effectively denatured during boiling due to high thermostability. This phenomenon could result in non-palindromic enrichment during GAPF.[38] Because of these technical issues, we excluded 1 kb bins consistently enriched in both tumor and normal GAPF samples (75,765 bins, ~2.5% of the entire 3,209,513 bins) to focus on identifying tumor-specific *de novo* DNA palindromes (**Supp Table 2**).

The remaining 3,133,748 bins were then arranged in descending order based on their read depth coverage. The observation that HCBs were tumor-specific (**Fig. 2C**) prompted us to investigate differential calling between tumor and normal DNA using the chromosomal distribution of the top 1,000 HCBs, visualized as GAPF profiles in pie charts (**Fig. 3A**). The examination of normal DNA GAPF profiles revealed HCBs originating from every chromosome (**Fig. 3B, Supp Fig. 4 and 5, Supp Table 3**). In contrast, tumor GAPF profiles exhibited HCBs primary originating from one or a few chromosomes, suggesting the potential clustering of *de novo* palindromes in the breast tumor DNA. The nearly uniform distribution of HCBs across all chromosomes in the normal GAPF profiles suggests the randomness of residual dsDNA after denaturation that were amplified before sequencing, as expected in a sample lacking *de novo* palindromes in single-copy regions of the genome. We also confirmed that GAPF profiles were highly reproducible (**Fig. 3C, Supp Fig. 6**).

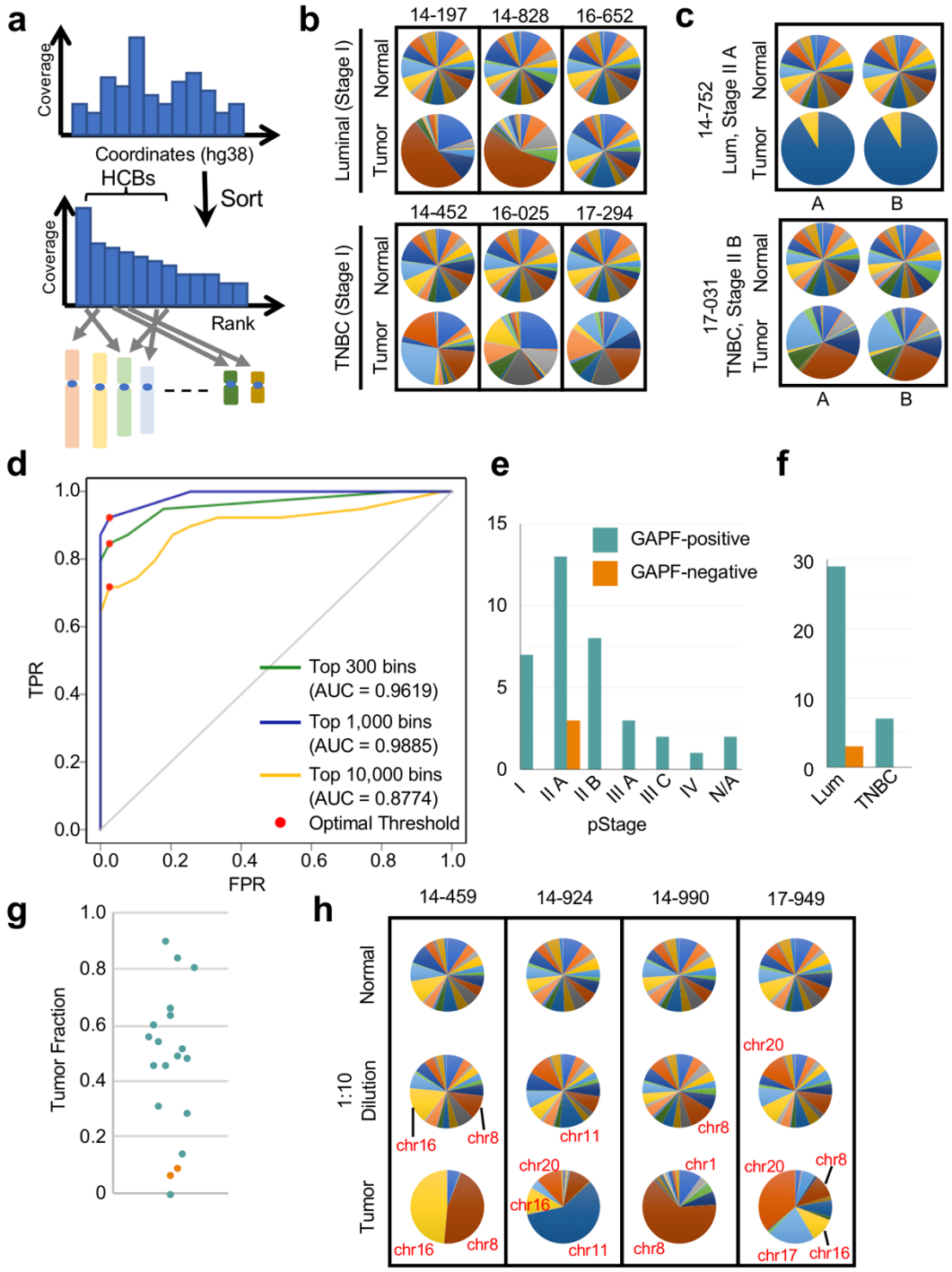

Fig. 3: High coverage GAPF bins classifies tumor or normal DNA using a threshold model. **a** The GAPF-seq analytical approach sorts 1 kb bins in descending order according to the normalized read coverage and identifies the chromosome of origin for the high coverage bins (HCBs) included in subsequent analyses. **b** GAPF profiles for breast tumors and matched normal buffy coat are visualized in pie charts, highlighting clustering of the top 1,000 HCBs on chromosomes. **c** GAPF profiles using the top 1,000 HCBs are reproducible as visualized in pie charts for two breast tumor pairs performed in duplicate. **d** Receiver operating characteristic (ROC) curves generated by varying the threshold for the number of HCBs on a chromosome as the classification criterion for tumor or normal DNA. The top 300 (green), 1,000 (blue), or 10,000 (orange) HCBs are considered. The optimal threshold (red dot) is determined by Youden's J statistic which maximizes sensitivity and specificity. **e** GAPF classification results for 39 breast tumors by stage using a chromosome threshold of 100 HCBs. **f** GAPF classification results for 39 breast tumors by subtype using a 100 HCB threshold. **g** Dot plot showing the tumor fraction (TF) by GAPF classification (blue = GAPF-positive, orange = GAPF-negative). n = 19. **h** GAPF profiles for normal DNA (top row), tumor DNA diluted 10x by normal DNA (middle row), and tumor DNA (bottom row).

The noticeable tumor-specific clustering of HCBs on chromosomes hinted at the intriguing possibility of identifying a global threshold for classifying samples as tumor or normal (threshold model).

To assess the optimal number of HCBs for effectively differentiate tumor and normal DNA, we generated receiver operating characteristic (ROC) curves using the top 300, 1,000, or 10,000 HCBs and evaluated their chromosomal distribution (**Fig. 3C, Supp Table 3, 4,** and **5**). The classification criterion for

determining whether a sample contains tumor DNA (GAPF-positive) or not (GAPF-negative) relied on whether HCBs exceeded a global threshold on any single chromosome. For the top 1,000 bins, the global threshold tested ranged from 70, classifying every sample as GAPF-positive, to 915, classifying every sample as GAPF-negative. The average area under the ROC curve (AUC) for the binary classifier using the top 1,000 HCBs was 0.9819 (s.d. $\pm$ 0.0249) with three-fold cross-validation and three different random assignment seeds. The optimal global threshold was then determined using Youden's J statistic, aiming to maximize the sensitivity and specificity of the binary classifier. Using the top 1,000 bins, the optimal threshold was determined to be 100 bins, achieving a sensitivity of 94.02% (s.d. $\pm$ 2.96%) and a specificity of 99.15% (s.d. $\pm$ 1.48%). Using the top 300 or 10,000 HCBs instead yielded AUC values of 0.9628 (s.d. $\pm$ 0.0266) and 0.9050 (s.d. $\pm$ 0.0556), respectively, indicating the top 1,000 as the most effective HCB group for the binary classifier in this dataset.

Using the top 1,000 HCBs and the threshold model, we identified 36 GAPF profiles with at least one chromosome above the 100-bin threshold (GAPF-positive), while 3 tumors were misclassified as normal (GAPF-negative) (**Fig. 3D**). Notably, the clustering of HCBs on a chromosome was evident for all stage I tumors (TNBC or luminal), demonstrating that GAPF-seq was capable of detecting early-stage breast cancers (**Fig. 3B, Fig. 3D**). The three GAPF-negative samples were all stage II A luminal breast tumors. Luminal tumors typically exhibit fewer SVs than TNBC,[43] which may explain GAPF-negative cases. As SVs often manifest as CNA, we quantified CNA for 31 breast tumors using shallow WGS and ichorCNA, a tool for estimating tumor fraction (TF) in plasma cell-free DNA (**Fig. 3G**). GAPF-negative tumors showed low CNA; however, several samples with low CNA were GAPF-positive (14-604, 16-094, and 16-263). To further examine whether GAPF-seq could call tumor DNA for tumors with very low CNA, we ran GAPF-seq with 10-fold *in vitro* dilutions of tumor DNA with paired normal DNA. All samples yielded the expected tumor DNA content after 10-fold dilution of tumor DNA. Based on the threshold model (**Fig. 3C**), seven out of 8 samples were accurately classified as tumor DNA, indicating that GAPF profiles have the potential to identify tumors with low DNA content (**Fig. 3H, Supp Fig. 7, Supp Table 6**).

Subtype-specific Clustering of High Coverage Bins

By examining chromosomes frequently carrying top 1,000 HCBs above the threshold, chr1 and chr8 appeared to be common between luminal and TNBC subtypes, while chr16 and chr11 were unique to luminal

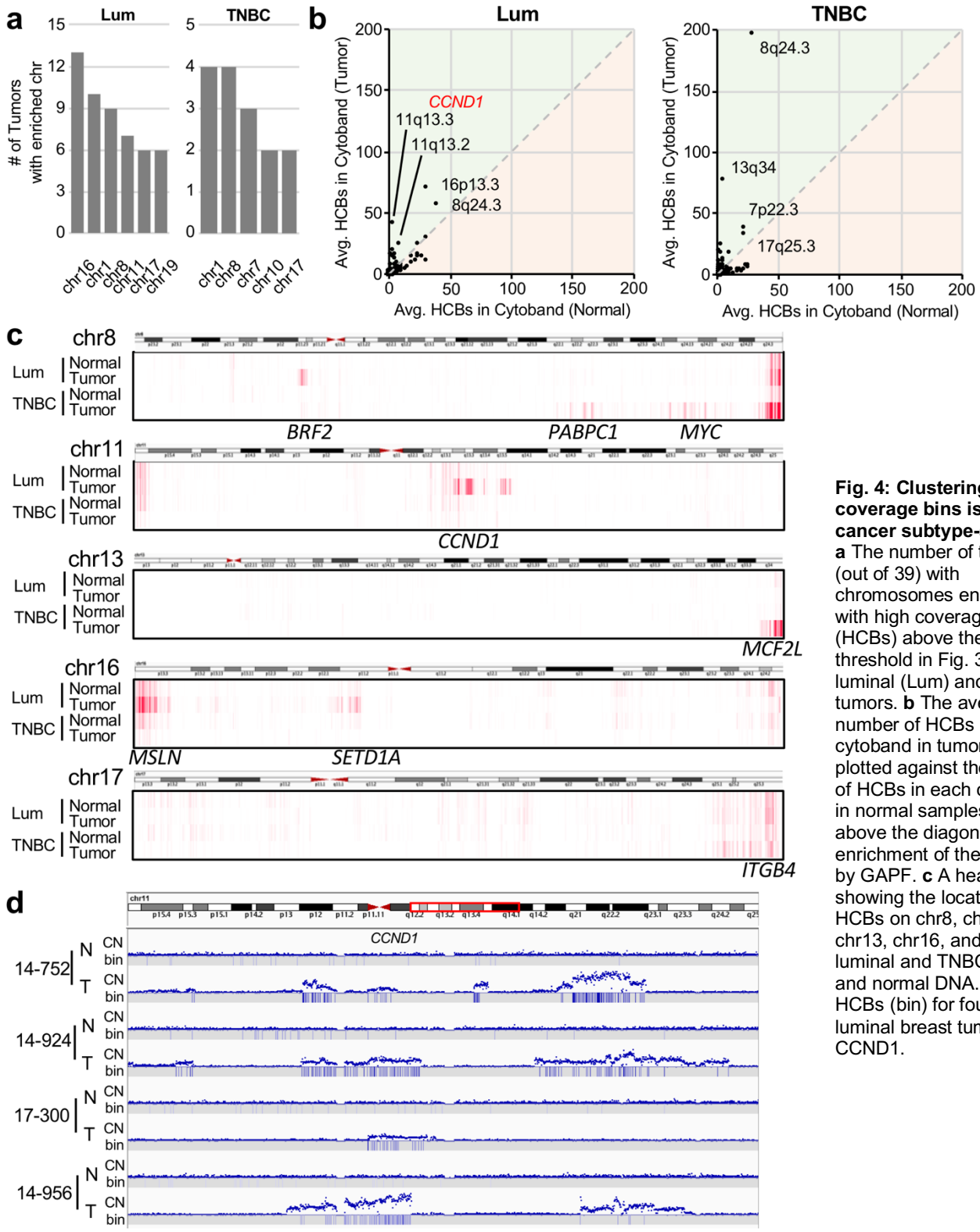

Fig. 4: Clustering of high coverage bins is breast cancer subtype-specific. **a** The number of tumors (out of 39) with chromosomes enriched with high coverage bins (HCBs) above the threshold in Fig. 3D for luminal (Lum) and TNBC tumors. **b** The average number of HCBs in each cytoband in tumors is plotted against the number of HCBs in each cytoband in normal samples. Points above the diagonal indicate enrichment of the cytoband by GAPF. **c** A heatmap showing the location of HCBs on chr8, chr11, chr13, chr16, and chr17 for luminal and TNBC tumor and normal DNA. **d** CN and HCBs (bin) for four (4) luminal breast tumors near CCND1.

and chr7 was unique to TNBC (**Fig. 4A**). We further investigated HCBs at the cytoband level, comparing the number of GAPF top 1,000 HCBs in each cytoband from tumor GAPF profiles to that of normal GAPF profiles (**Fig. 4B**). In TNBC, on average 197.6 of 1,000 HCBs were in 8q24.3, the telomeric end of 8q, in contrast to 28.0 HCBs in normal DNA. The 8q24.3 cytoband was also a hotspot for enrichment in luminal tumor DNA and,

to the lesser extent, in normal DNA (**Fig. 4C**). HCBs were often clustered in cytobands close to telomeres. In addition to 8q24.3, clustering was observed in the telomeric cytobands 13q34 (in TNBC) and 16p13.3 (in luminal) in a tumor subtype-specific manner (**Fig. 4B, Fig. 4C**). The fusions of critically short telomeres followed by BFB cycles[46] may underlie the enrichment of palindromes and HCBs at the cytobands of chromosome ends. Notable exceptions include cytobands 8q24.21 (in TNBC) and 11q13.2-5 (in luminal), which house prevalent breast cancer oncogenes *MYC* and *CCND1*, respectively, and are frequently amplified. Indeed, the amplification of the *CCND1* locus was strongly associated with HCBs (**Fig. 4D**). Complex CNA patterns at 11q13 were common in luminal, with another amplicon telomeric to the *CCND1* amplicon associated with HCBs.

Aberrant read pairs spanning palindromic junctions are likely underrepresented,[41,42] and deep coverage would be necessary to identify FF or RR read pairs (**Fig. 1D**). Nonetheless, we identified multiple RR read pairs at the copy number breakpoint of the amplicon at 11q13.2 with HCBs clustering nearby (**Supp Fig. 8**).

Machine Learning Algorithms for Binary Classification

Aside from the Youden's J statistic-based threshold model for our dichotomous diagnostic test, a variety of statistical, probabilistic, and optimization techniques can be applied to genomic data using machine learning (ML) for binary classification. An automated end-to-end ML pipeline called STREAMLINE[47] was used for the binary classification of the breast tumor and paired normal DNA (as in **Fig. 3**). The number of top 1,000 HCBs on each chromosome from the GAPF-seq data was input as a two-dimensional array and STREAMLINE attempted to identify the samples as tumor or normal DNA. STREAMLINE, a recently developed AutoML tool, facilitates ML modeling by enforcing rigorous modeling algorithm comparisons, analysis transparency, reproducibility, and sensitivity to complex associations in data. In the first year of its release it has been successfully applied to various biomedical ML modeling and data mining tasks.[48,49] After basic data cleaning and three-fold cross-validation partitioning (**Fig. 5A**), ML models were trained using Naïve-Bayes (NB), random forest (RF), extreme gradient boosting (XGB), category gradient boosting (CGB), and extended supervised tracking and classifying system (ExSTraCS) algorithms. All models yielded very high AUC values (**Fig. 5B**). To minimize batch effects from partitioning, the ML modeling was repeated using two additional random assignment seeds, and the AUC results from all three seeds were averaged (**Fig. 5C**). Average AUC values

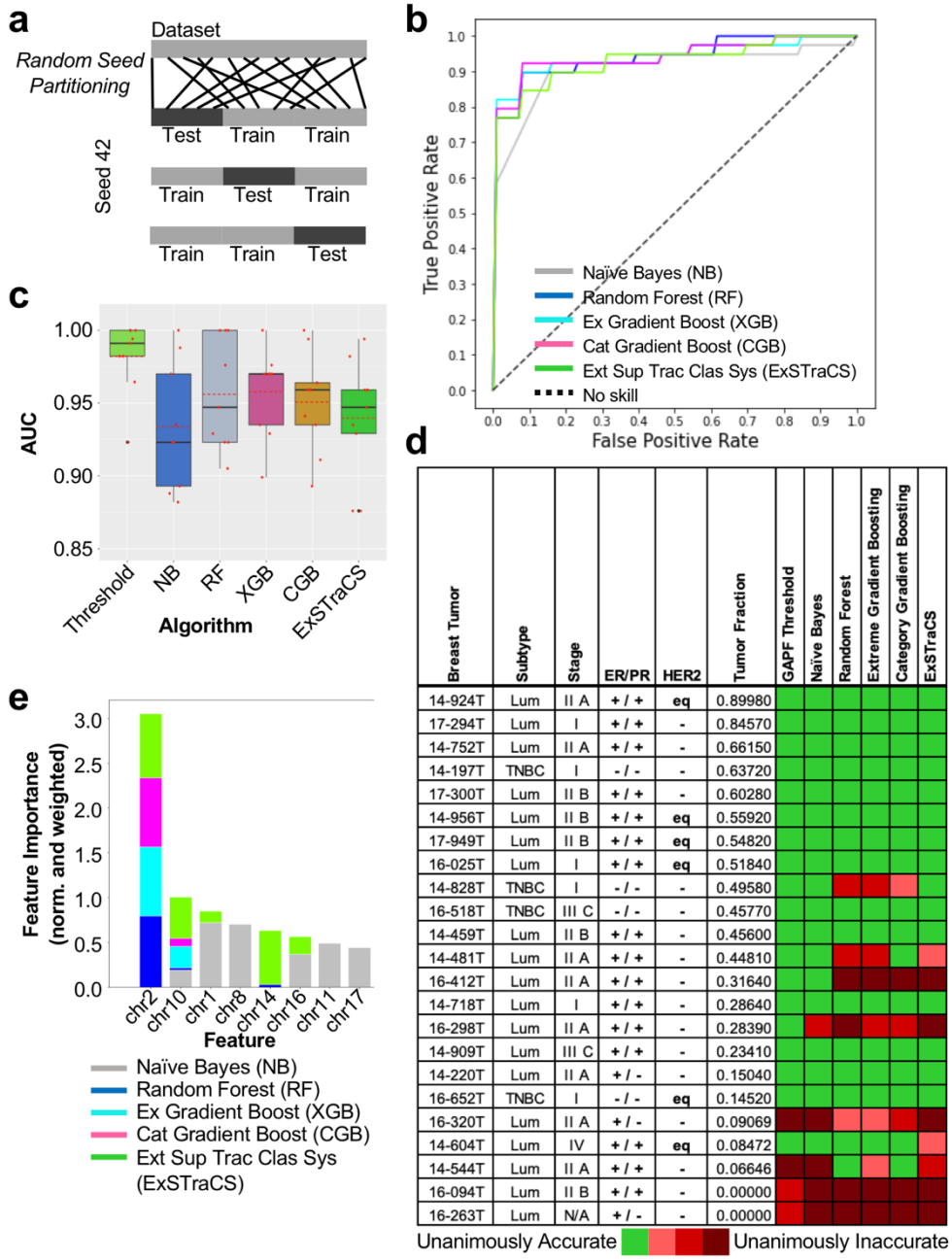

Fig. 5: A machine learning pipeline with GAPF-seq accurately classifies tumor and normal DNA.
a Random seed partitioning of the dataset assigns data points into groups for cross-validation (CV) testing of modeling. In three-fold CV, two groups are used to train the model while the remaining group is used to test the model. **b** ROC curves for machine learning (ML) models generated by STREAMLINE classifying tumor or normal DNA using the Naïve-Bayes (NB), random forest (RF), extreme gradient boosting (XGB), category gradient boosting (CGB), and extended supervised tracking and classifying system (ExSTraCS) algorithms with a random assignment seed of 42 and three-fold CV. **c** Box plots showing the AUC from each of 3 cross-validation testing sets for models generated using random assignment seeds of 22, 32, and 42. Red dot = AUC value, red dotted line = mean AUC. **d** Table of breast tumor subtype, stage, ER/PR/HER2 status, and tumor fraction (TF) with a heatmap showing the congruence of classification results from random assignment seeds and the threshold and machine learning (ML) models. **e** Composite normalized and weighted feature importance bar plots. Scores are normalized within each algorithm and weighted by the median AUC for that algorithm. Composite importance bar plots normalize feature importance scores within each algorithm and then weights these normalized scores by the median AUC for that algorithm to consider accurate models more than less accurate ones.

were greater than 0.93 for all models, with the XGB model demonstrating the highest performance (Avg. AUC = 0.958). Each unique seed yielded a predicted class for a sample, and a heatmap visualized the congruence of true positive outcomes (**Supp Table 7**). Binary classification was generally consistent among models, with a few exceptions (**Fig. 5D**). An improvement over the threshold model was observed in calling 14-544T, correctly called by RF and CGB models, which was particularly notable given that tumors with low TF were often mis-classified as GAPF-negative, as in **Fig. 3G**. Conversely, several non-linear prediction models incorrectly classified 14-828T, 16-412T, and 16-298T as GAPF-negative.

The STREAMLINE ML pipeline also provided the estimation of the relative importance of each chromosome in accurately predicting tumor or normal DNA based on the GAPF profile (**Fig. 5E**). Feature importance was determined by randomly permutating one chromosome at a time in the testing data and evaluating its impact on the performance of each ML model.[50] Interestingly, non-linear classification models RF, XGB, CGB, and ExSTraCS all deemed chr2 as most important. Specifically, RF and CGB based their models predominantly on chr2, which contrasts with our threshold model. All of the top five chromosomes (chr2, chr10, chr14, chr15, chr18) deemed important for binary classification by RF, XGB, CGB, and ExSTraCS, exhibited depletion in tumor GAPF profiles relative to normal profiles. For example, normal samples had an average of 51.3 of the top 1,000 HCBs on chr2 whereas tumor tissue had only 24.3 (**Supp Table 3**). In contrast, for chromosomes frequently carrying HCBs above the threshold such as chr8 and chr11, the average numbers of HCBs were 51.3 and 64.8 in normal and 135.9 and 121.2 in tumor, respectively. Only the linear classifier algorithm Naïve-Bayes yielded high feature importance scores for chr1, chr8, and chr11, all of which were frequently above the threshold determined by Youden's J statistic.

Long cfDNA Fragments and Tumor Fraction

With the ability to differentiate tumor DNA from paired normal DNA, we proceeded to evaluate GAPF-seq using plasma-borne cfDNA (cfGAPF-seq). GAPF-seq presumably relies on sufficiently long DNA fragments to ensure that both arms of DNA palindromes are physically tethered together in a continuous fragment, facilitating intra-strand annealing by snap-back. However, prevalent methods for extracting cfDNA from plasma employ affinity-columns or -beads and predominantly yield fragments bound to mono- or di-nucleosomes, which would be too short to capture palindromes. Whether very long circulating tumor DNA (ctDNA) fragments exist in the plasma of cancer patients remains a topic of debate.[51] To investigate whether long cfDNA fragments exist and are as feasible for cancer detection as short cfDNA fragments, we isolated cfDNA using 0.5 mL plasma from 10 advanced prostate cancer (PCa) patients using either affinity-beads or traditional phenol-chloroform extraction (PCE) (**Fig. 6A**). Plasma from advanced prostate cancer (PCa) patient is expected to carry sufficient ctDNA for analyses whereas the majority of our breast tumor samples are Stage II or earlier and less likely to have high amounts of ctDNA in plasma. Additionally, the use of PCa cfDNA serves as an initial test for GAPF-seq as a pan-cancer approach. The bead-based cfDNA isolation kit yielded

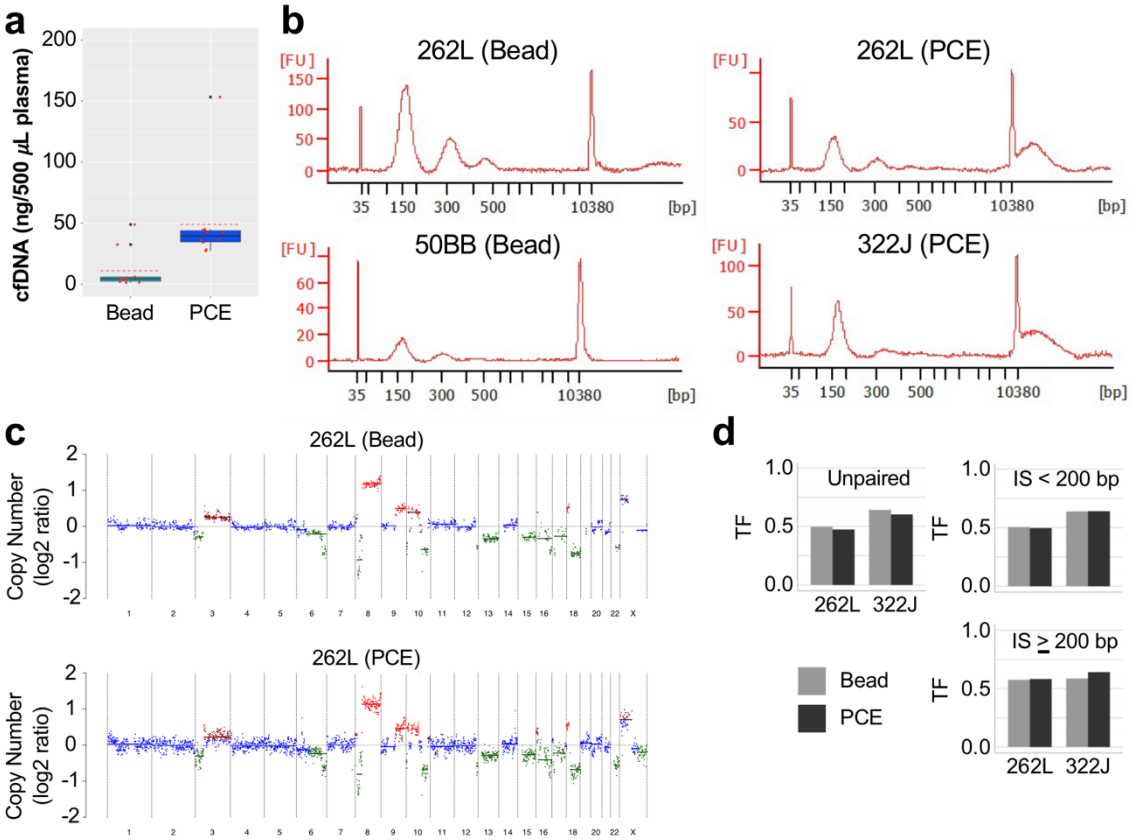

Fig. 6: Long fragment cell-free DNA (cfDNA) extracted from plasma contains circulating-tumor DNA (ctDNA). **a** The amount of cell-free DNA (cfDNA) extracted from plasma of prostate cancer (PCa) patients using affinity-bead based extraction (bead) (n = 10) or phenol-chloroform extraction (PCE) (n = 10) normalized to 500 μL plasma. Red dotted line = mean. **b** Fragment analysis of cfDNA isolated from the blood of PCa patients using affinity-bead based extraction (bead) or phenol-chloroform extraction (PCE). **c** Copy number (CN) of cfDNA extracted using affinity beads (bead) or PCE as calculated by ichorCNA. **d** Tumor fraction (TF) for PCa cfDNA using unpaired sequencing reads (left) and paired sequencing reads with short (<200 bp) (top right) and long (>200 bp) (bottom right) insert sizes (IS).

an average of 11 ng of cfDNA per 500 μL of plasma, with only two samples yielding more than 10 ng. In contrast, PCE yielded 49 ng on average with at least 27 ng from every sample. Due to the low amount of cfDNA extracted by the bead-based isolation kit, there was often insufficient cfDNA for additional characterization experiments beyond sequencing. Furthermore, whereas the bead-based cfDNA isolation kit yielded mono-, di-, and even some tri-nucleosomal cfDNA, PCE extraction resulted in a broad range of cfDNA fragment sizes, including nucleosome-sized fragments (**Fig. 6B**). Notably, fragments longer than 10 kb were observed, which would be amenable to snap-back. We then used fragmentation and NGS library construction for shallow WGS to evaluate TF using ichorCNA. Patterns in CNA patterns appeared similar between affinity bead-extracted and PCE cfDNA (**Fig. 6B** and **Fig. 6C**). Slightly lower TF was observed in PCE cfDNA extracted from either 262L or 322J. To examine whether the decreased TF was due to lower TF in long fragments of the library, we evaluated TF for paired sequencing reads with short (<200 bp) and long (≥200 bp) insert sizes (**Fig. 6D**), assuming that read pairs with >200 bp insert sizes likely originated from long DNA

fragments after fragmentation rather than mononucleosomal fragments. TF was equally represented in both populations of size-selected reads, indicating that long cfDNA fragments would also be feasible for cancer detection.

High Coverage Bins on chrX as a Determinant of Binary Classification

GAPF profiles with the top 1,000 HCBs were generated from cfDNA along with matched leukocyte DNA from the buffy coat from 10 PCa patients (**Fig. 7A, Supp Fig. 9, Supp Table 8**). Similar to the GAPF profiles from breast tumor and buffy coat DNA, HCBs from normal DNA were distributed across every chromosome. In contrast, PCa cfDNA exhibited modest clustering of HCBs. An ROC curve using the top 1,000 HCBs showed that the AUC was 0.887 (s.d. ± 0.131) (**Fig. 7B**). The optimal global threshold determined by Youden's J statistic was 90 bins, resulting in a sensitivity of 87.04% (s.d. ± 15.65%) and a specificity of 79.63% (s.d. ± 21.29%). TF was determined for each cfDNA using shallow WGS and ichorCNA, and were grouped based on this output from GAPF profiles by our threshold model (**Fig. 7C**). All 5 samples with TF>0.1 were all correctly called GAPF-positive. The single false negative sample (353B) did not have the lowest TF, and two samples (324D and 213I) were correctly classified as GAPF-positive despite an estimated tumor fraction of zero. STREAMLINE was then used to generate binary classification models. The AUC values from each cross-validation set from 3 seeds were averaged together. The best-performing model, on average, utilized the NB algorithm (Avg. AUC = 0.905) (**Fig. 7D**). A heatmap visualized the congruence of true positive outcomes against the castration status, prostate-specific antigen (PSA) level prior to treatment, and TF of PCa cfDNA (**Fig. 7E, Supp Table 9**). Increased PSA and TF correlated with more accurate classification by cfGAPF-seq and castration resistance.

Considering that plasma cfDNA and DNA extracted from the buffy coat underwent different pre-analytical steps, it’s essential to address whether the binary classification results could potentially be influenced by differences in sample processing. To investigate this issue, cfGAPF-seq was performed on 11 plasma samples obtained from males without any known diseases (**Fig. 7F, Supp Fig. 10, Supp Table 10**). These healthy "normal" plasma samples were classified alongside the 10 plasma samples from PCa patients using ML modeling. The average AUC values from three different models for each algorithm were averaged, and the best-performing model utilized the CGB algorithm (Avg. AUC = 0.965) (**Fig. 7G**)

.

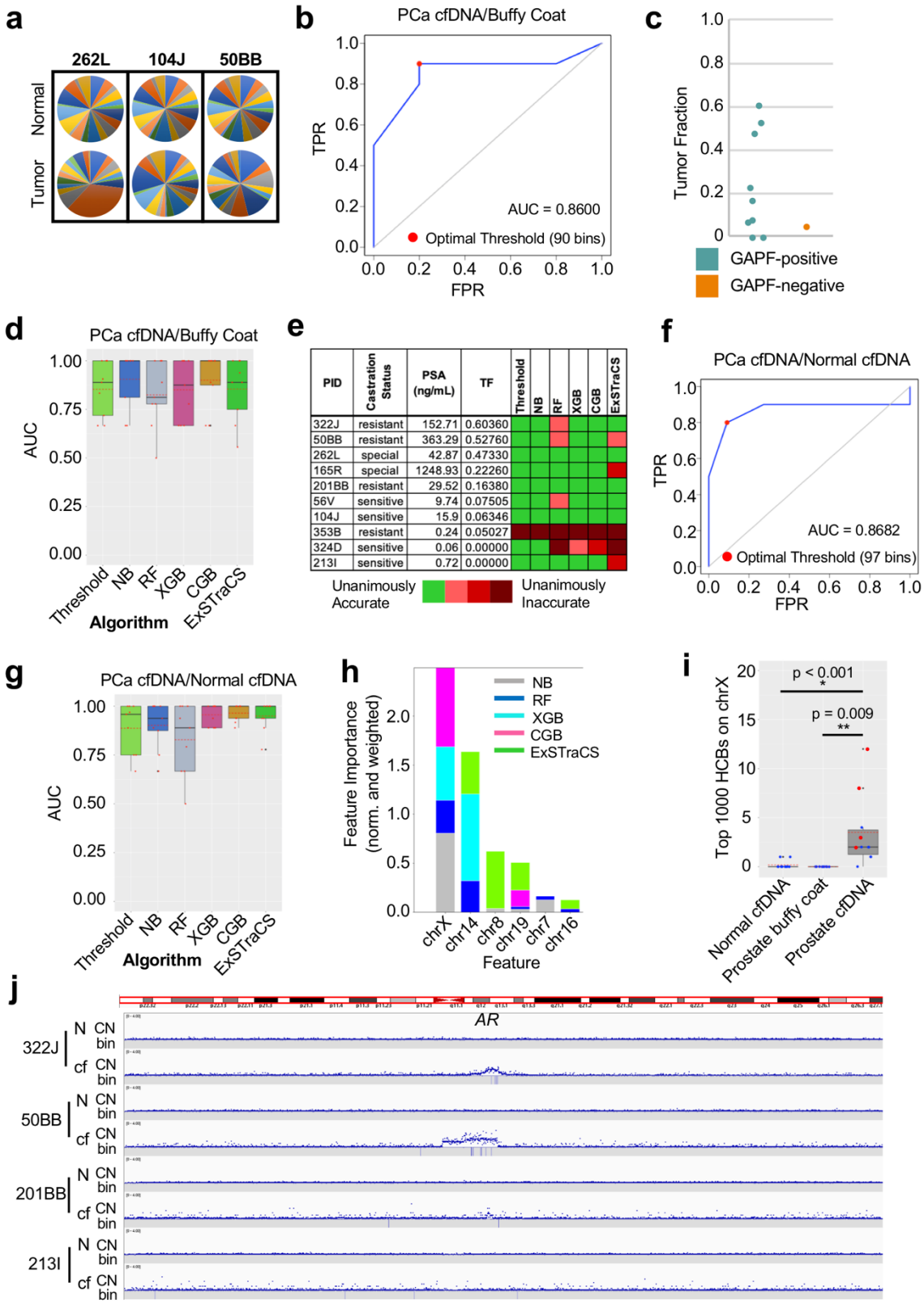
a
262L
104J
50BB
Normal
Tumor
b
PCa cfDNA/Buffy Coat
TPR
FPR
AUC = 0.8600
Optimal Threshold (90 bins)
c
Tumor Fraction
GAPF-positive
GAPF-negative
d
PCa cfDNA/Buffy Coat
AUC
Threshold
NB
RF
XGB
CGB
ExSTraCS
Algorithm
e
PID
Castration Status
PSA (ng/mL)
TF
Threshold
NB
RF
XGB
CGB
ExSTraCS
322J resistant 152.71 0.60360
50BB resistant 363.29 0.52760
262L special 42.87 0.47330
165R special 1248.93 0.22260
201BB resistant 29.52 0.16380
56V sensitive 9.74 0.07505
104J sensitive 15.9 0.06346
353B resistant 0.24 0.05027
324D sensitive 0.06 0.00000
213I sensitive 0.72 0.00000
Unanimously Accurate
Unanimously Inaccurate
f
PCa cfDNA/Normal cfDNA
TPR
FPR
AUC = 0.8682
Optimal Threshold (97 bins)
g
PCa cfDNA/Normal cfDNA
AUC
Threshold
NB
RF
XGB
CGB
ExSTraCS
Algorithm
h
Feature Importance (norm. and weighted)
NB
RF
XGB
CGB
ExSTraCS
chrX
chr14
chr8
chr19
chr7
chr16
Feature
i
Top 1000 HCBs on chrX
p < 0.001
*
p = 0.009
**
Normal cfDNA
Prostate buffy coat
Prostate cfDNA
j
AR
322J
50BB
201BB
213I
N CN bin
cf CN bin

Fig. 7: GAPF-seq accurately classifies PCa cfDNA and points to chrX as a key determinant factor.
a GAPF profiles using the top 1,000 high coverage bins (HCBs) of prostate cancer (PCa) cfDNA and matched buffy coat DNA visualized in pie charts. **b** ROC curve generated by varying the threshold for the number of top 1,000 HCBs on a chromosome as the classification criterion for PCa cfDNA or normal buffy coat DNA. The optimal threshold (red dot) is determined by Youden's J statistic. **c** Dot plot showing the tumor fraction (TF) by GAPF classification (blue = GAPF-positive, orange = GAPF-negative) (n = 10). **d** Box plots of AUC values for classifying PCa cfDNA and matched buffy coat DNA for machine learning (ML) classifiers using the Naïve-Bayes (NB), random forest (RF), extreme gradient boosting (XGB), category gradient boosting (CGB), and extended supervised tracking and classifying system (ExSTraCS) algorithms with three-fold CV and random assignment seeds of 22, 32, and 42. Red dot = AUC value, red dotted line = mean AUC. **e** Table showing the PCa castration status, PSA (ng/mL), and tumor fraction (TF) with a heatmap of the congruence of classification results from random assignment seeds of 22, 32, and 42 and different classification models. **f** ROC curve for PCa cfDNA or healthy male cfDNA. The optimal threshold (red dot) is determined by Youden's J statistic. **g** Box plots of PCa cfDNA and cfDNA from healthy male individuals showing the AUC from testing sets for models generated using random assignment seeds of 20, 32, and 42. Red dot = AUC value, red dotted line = mean AUC. **h** Composite normalized and weighted feature importance bar plots. Scores are normalized within each algorithm and weighted by the median AUC for that algorithm. **i** Box plots showing the number of top 1,000 HCBs on chrX for GAPF-seq data using healthy male cfDNA (n = 11), buffy coat DNA from PCa patients (n = 10), and cfDNA from PCa patients (n = 10). * $p < 0.001$, two-sided Wilcoxon rank-sum test. ** $p = 0.009$, Wilcoxon signed-rank test. Red dot = AUC value, red dotted line = mean AUC. **j** CN and HCBs (bin) for PCa cfDNA on chrX near the androgen receptor gene (AR).

As for the feature importance, models using NB, RF, XGB, and CGB all identified chrX as the first or second most important feature for binary classification (**Fig. 7H**). Because none of the samples had a seemingly significant number of top 1,000 bins on chrX, our threshold-based calling was insensitive to chrX. Therefore, we independently evaluated chrX HCBs in calling tumor cfDNA (**Fig. 7I**). While zero or one top 1,000 HCBs cfDNA were on chrX from healthy individuals or buffy coat DNA from PCa patients, quite a few of HCBs were mapped to chrX in cfDNA from PCa patients. Indeed, HCBs on chrX were statistically different between PCa cfDNA and either matched normal DNA ($p < 0.001$, Wilcoxon signed-rank test) or healthy individuals' cfDNA ($p = 0.009$, two-sided Wilcoxon rank-sum test).

Given that the androgen receptor gene (AR) is located on chrX and contributes to therapy-resistance in advanced PCa[52-54], we examined AR amplification (AR-amp) through shallow WGS. AR-amp was notable in four patients with therapy-resistant tumors and very high PSA, with dozens of top 1,000 bins within the amplified regions (**Fig. 7J**). In other patients, AR-amp was not evident, and HCBs were fewer and scattered throughout chrX. These PCa cases were therapy-sensitive at the time of the blood draw but would eventually progress to resistance and life-threatening disease. HCBs on chrX, as assessed by cfGAPF-seq, could be an initial sign of chrX-wide rearrangement that would eventually leads to AR-amp, which could be consistent with DNA palindrome formation as an initial step of gene amplification.

Discussion

In this study, we tested the feasibility of our genome-wide assay, named cfGAPF-seq, which targets DNA palindromes, for liquid biopsy-based cancer detection. DNA palindromes are mechanistic components of

BFB cycles, which were shown to be a major process underlying genome instability and genomic amplification across tumor types.[36] Consequently, targeting DNA palindromes for cancer detection seemed a rational strategy to test. GAPF is designed to enrich DNA palindromes and eliminate non-palindromic DNA. This feature would enable cfGAPF-seq to detect cancer-specific DNA with high sensitivity in plasma cfDNA even with low tumor fraction (TF). To validate this concept, we conducted experiments using samples with *in vitro* serial dilution of tumor DNA mixed with normal DNA as well as cfDNA with various TFs.

If developed as a cancer detection test, GAPF-seq would be uniquely positioned for liquid biopsy targeting SVs. While WGS and mate-pair analyses of tumor DNA can successfully identify fold-back inversions,[31,55] it requires substantial coverage (>30x). In cfDNA, DNA representing fold-back inversions is diluted, which would demand ultra-deep coverage for accurate detection. However ultra-deep WGS is cost-prohibitive and requires significant time and effort for analyses. Targeted sequencing for gene mutation detection in cfDNA would offer a higher sensitivity for cancer detection, as exemplified by detecting tumor-informed mutations.[56,57] However, many amplified oncogenes lack mutations. Gene amplification is not limited to treatment-naïve primary tumors for activating oncogenes; it also occurs later during disease progression to confer therapy resistance, information that is absent in primary tumors. Therefore, mutation detection tests are not feasible for the early detection of gene amplification conferring therapy resistance. Early detection of resistance would allow physicians to consider treatment options when resistant tumors are still small. Thus, frequent monitoring through liquid biopsy and timely detection of gene amplification is important. GAPF-seq with simple cfDNA processing, low coverage NGS, and streamlined data analysis would emerge as a practical approach for frequent monitoring.

The proof of concept was tested in this study for the Androgen receptor gene amplification (AR-amp) in lethal prostate cancer (PCa). AR-amp is very often associated with advanced PCa.[54] AR signaling is a major driver of PCa progression. Contemporary AR signaling inhibitors such as enzalutamide, apalutamide, abiraterone have significantly improved the overall survival of patients in recent years.[58,59] Despite these advancements, resistance eventually develops, leading to metastasis and lethal disease. The only clinical indication of resistance is a rising PSA. Given accumulating data advocating the benefits of early initiation of chemotherapy, a test indicating resistance to AR suppression early would provide an opportunity to alter the

therapeutic approach, potentially leading to improved survival.[52] We found that genomic regions enriched by cfGAPF-seq on X chromosomes (chrX) were almost exclusively seen in PCa plasma cfDNA (**Fig. 7I**): all four cases with anti-AR therapy resistance and five out of six therapy-sensitive cases. Resistance cases were characterized by high TF in cfDNA and AR-amp (**Fig. 7J**). These results suggest that palindrome formation and BFB cycles underlie AR-amp. The other six cases did not show AR-amp; however, high coverage bins (HCBs) scattered throughout chrX. Such bins may be early signs of BFB cycles and chromosome-wide rearrangements that could eventually lead to AR-amp. If this hypothesis holds true, these patients are likely to develop AR-amp over time. If not, HCBs on chrX could be a simple indicator of cancer DNA. A comprehensive study involving longitudinally collected early and late-stage samples would distinguish these two possibilities.

We utilized chromosomal distributions of high coverage bins (HCBs, GAPF profiles) as outputs from GAPF-seq to test their efficacy in distinguishing breast tumor DNA samples from normal DNA and PCa patients' cfDNA from normal DNA or healthy individuals' cfDNA. While the output performed well in most cases, several breast tumor (luminal) DNA and at least one PCa cfDNA were inconsistently classified. It was noted that all of these cases exhibited low copy number alterations (CNA) levels or TF measured by ichorCNA. This suggests the possibility that tumor-derived DNA was very rare in these samples. This is most likely the case for PCa cfDNA because disease burden, estimated by PSA, was low for the inconsistently classified or GPAF-negative cases. Another potential explanation is that GAPF-seq profiles are not a robust measure of tumor DNA when chromosomal rearrangements are rare. In this regard, all three GAPF-negative cases were from luminal tumors, which are known to be driven by hormone-dependent signaling.[60] Understanding the discriminative power of GAPF-seq to differentiate tumor DNA from normal DNA for each tumor tissue of origin would thus be necessary.

Relatively straightforward threshold approach yielded superior binary classification results in terms of AUC to many ML models (**Fig. 5C**). In contrast to the ML models, which exclusively utilize HCBs as input data, the simple threshold models have the advantage of incorporating domain knowledge. This includes recognizing that (1) a burden count above some threshold may be informative and (2) there is an informative higher-level feature abstraction (i.e., one or more chromosomes have a burden above the target threshold). In order for ML algorithms to train a model similar to the threshold models, it would need to first learn the abstract concept

which decides "IF" any of the HCB features in the dataset have a value over a target threshold. The challenge of this abstraction is reflected in long standing computer science benchmark problems such as the "majority-on" or "even-parity" problems where simultaneous knowledge of multiple features values is required to solve the problem (i.e., the majority of features in a set above some threshold, or the sum of feature values in a set is even, respectively).[61,62] This ML challenge can be addressed in future work via feature engineering; applying domain knowledge to construct new features that capture information across all chromosomes (e.g. construct a binary feature identifying if any chromosome in the dataset has HCBs above a given threshold). This would be expected to improve ML binary classification. Beyond feature engineering, additional opportunities to improve the predictive performance of GAPF-seq with ML include (1) utilizing more sophisticated ML algorithms, (2) conducting a more extensive optimization of algorithm hyperparameters, and (3) combining base models trained by different ML algorithms into a predictive ensemble.

The decision to employ chrX-based tumor/normal differentiation for PCa cfDNA/normal DNA was guided by insight from ML (**Fig. 7I**). Due to the scarcity of HCBs on chrX, none of the cfDNA samples reached the threshold. Nevertheless, the assessment of feature importance unveiled that ML algorithms strongly relied on HCBs on chrX for binary classification (**Fig. 7H**). Consequently, ML highlighted a feature that human observers (i.e., the authors) had not considered. Feature importance stands out as a widely used technique to elucidate the behavior of ML models, and its significance is particularly pronounced in the medical field.[63] The importance of DNA palindromes on chrX is easily interpretable, given that AR-amp is a primary driver of resistance to therapy.[52-54] These results suggest that cfGAPF-seq, when employing threshold model, has limitations, and the full potential of cfGAPF-seq for calling tumor DNA has not been exhausted. Increasing the number of samples in future studies will enable us to enhance the analysis pipeline. Additionally, elevating the resolution of HCB positioning in 1,293 cytobands genome-wide may offer a more comprehensive assessment. For example, cfDNA fragmentation patterns were examined in 504 windows of 5 Mb genome-wide.[23,24] DNA methylation profiling used over 1 million CpG sites in the genome, the methylation patterns of which best predict the tissue of origin and differentiate tumor DNA from normal DNA.[64] The substantial computational power required for such analyses can be efficiently managed through the application of ML. Feature importance would then be instrumental in identifying hotspots of DNA palindromes at the cytogenetic level.

Limitations of the study

- While GAPF-seq has shown efficient differentiation between tumor DNA and normal DNA for breast tumors and prostate cancer patients' plasma, its applicability to other tumor types remains to be tested.
- HCBs in chrX seems definitive for calling circulating tumor DNA. Nevertheless, conducting studies with larger sample size is essential to establish a strong case.

Methods

Research Samples:

For mimicking DNA with low tumor DNA contents, we utilized the Colo320DM colorectal cancer cell line, which harbors known palindromic junctions[28] and IMR90 normal fibroblasts. Breast cancer patients' samples were obtained from the BioBank at Cedars-Sinai Medical Center, which stores matched frozen tumor/buffy coat/plasma samples. The project was approved by the Institutional Review Board (Pro0005127, DNA palindrome detection by liquid biopsy from breast cancer patients; 00042197 Translational Oncology Program Blood Specimen Repository). Human normal plasma from single donors was procured from Innovative Research.

DNA extraction:

High Molecular Weight DNA was extracted from cell lines and tissues as described previously.[41] Briefly, samples were incubated in 400 μL of lysis buffer (100mM NaCl, 10mM Tris, 25mM EDTA and 0.5% SDS) and 20 μL of Proteinase K (20 mg/mL) at 37 °C for 16 hours, followed by phenol/chloroform extraction and ethanol precipitation. Gene Jet Whole Blood DNA extraction kit (Thermo Scientific) was used to extract DNA from buffy coat. For plasma cfDNA extraction, a modified phenol-chloroform protocol was used. Frozen aliquots of 500 μL of plasma were thawed and mixed with 2.5 mL of cell lysis buffer and 200 μL proteinase K (20 mg/mL), followed by an incubation at 37°C for at least 16 hours. A phenol-chloroform-isoamyl alcohol mixture (Sigma-Aldrich) was added and mixed. The mixture was centrifuged at 10,000 g for 15 min and the aqueous portion was subject to a second phenol-chloroform treatment. A chloroform-isoamyl alcohol mixture ((Sigma-Aldrich) was then added and mixed, followed by centrifugation at 10,000 g for 15 min. To the aqueous portion, 0.05 mg of glycogen (Roche) and sodium acetate to a final concentration of 0.3 M were added. Then, 2:1 absolute

ethanol was added and kept at -20°C overnight. The mixture was centrifuged at 14,000 g for 30 min at 4°C and the pellet was washed with 70% ethanol before being resuspended in low TE buffer (Thermo Scientific). cfDNA concentration was measured using dsDNA HS Assay Kit and a Qubit 3.0 fluorometer (Life Technologies). DNA fragment analysis was performed using Agilent 2100 Bioanalyzer system (Agilent).

Genome-wide Analysis of Palindrome Formation:

For the analysis of small amounts of DNA, we devised a modified protocol of the Genome-wide Analysis of Palindrome Formation (GAPF)[38]. Briefly, either 100 ng or 30 ng of input genomic DNA was digested with either KpnI or SbfI, both of which are relatively infrequent cutting enzymes, at 37°C for 16 hr. The restriction enzymes were heat-inactivated at 65°C for 20 min and the reaction products were mixed. This mixture was boiled for 7 min in 100 mM NaCl and 50% formamide, then immediately quenched in ice water for 5 min. Subsequently, DNA was digested with 100 U/μg of S1 nuclease (Roche) at 37°C for 1 hour and was processed with the ChargeSwitch PCR Clean-up Kit (Invitrogen) or Monarch PCR and DNA Cleanup Kit (New England Biolabs).

The purified DNA was fragmented using the Covaris M220 and the libraries were constructed using the NEBNext Ultra II DNA Library Prep Kit (New England Biolabs) for next generation sequencing. Alternatively, GAPF libraries were constructed with the NEBNext Ultra II FS DNA Library Prep Kit (New England Biolabs), which employs fragmentase for DNA fragmentation. Whole-genome sequencing libraries were constructed using 40 ng of genomic DNA.

Whole Genome Sequencing:

All samples were sequenced on the Illumina HiSeq System by Novogene Co., Ltd. to generate 150 bp paired-end sequencing reads, achieving approximately 7.5x coverage. The reads underwent adaptor removal using Trim Galore (v0.6.1) and Cut Adapt (v2.3) (*trim galore options: --length 55*) and aligned to the UCSC hg38 human reference genome (hg38.fa.gz, 2014-01-15 21:14) using the DNA alignment software Bowtie 2 (v2.3.5) (*options: -x -U -S or -x -1 -2 -S*). The aligned reads were converted to binary format (*samtools view options: -bS*), reordered (*samtools sort options: -o*), and sorted (*sort options: -k1,1 -k2,2n -o*) using Samtools (v1.9) and counted in genome-wide 1 kb non-overlapping bins using Bedtools (v2.28.0) (*bedtools coverage options: -sorted -counts -a -b -g*). Coverage was visualized using the Integrative Genomics Viewer (IGV) (v2.5.0). Read counts were normalized by a per-million scaling factor to adjust for the sequencing depth.

GAPF-seq Quality Control:

To assess the quality of palindrome amplification by GAPF-seq, we examined the read coverage for known inverted repeats on chromosomes 1, 9, 17, 19, and X (Supp Table 11). These short inverted repeats are infrequently cut by the restriction enzymes and readily amplified by GAPF. Reads were counted at specific inverted repeats at the X chromosome genes DMRTC1, SSX2, SSX4, CXorf49, CXorf51A, PNMA6A, and SPANXA2 as well as the inverted repeats at HIST2H3C on chr1, FAM225A on chr9, SNORD3A on chr17, and 19p13.2. Normalized read counts for each of the regions were averaged to derive an amplification score. Because these regions are repeated within the reference genome, filtering based on mapping quality score that only returns reads that uniquely map to the reference genome should deplete the normalized read counts (*samtools view options: -b -q 40*). Thus, filtered values for each region were averaged to determine a depletion score. GAPF-seq passes quality control with an amplification score above 1.0 and a depletion score less than 0.075, which indicates the enrichment of DNA palindromes and elimination of non-palindromic or repeated sequences.

GAPF Background Bins:

Due to their repetitive structure, high GC content and epigenetic modifications, certain regions of the genome may yield false positives or obscure the identities of DNA palindromes.[38] To mitigate this, we first applied a filter based on mapping quality score (MAPQ > 40), retaining reads that uniquely map to the reference genome (hg38). Subsequently, we excluded regions that were commonly enriched in both tumor and normal samples. This curation resulted in 3,133,748 bins for further GAPF analysis, down from the original 3,209,513 non-overlapping 1 kb bins (Supp Table 2).

Cytoband Analysis:

Coordinates for cytogenetic bands in hg38 were downloaded from the UCSC genome browser (cytoBand.txt.gz, 2022-10-28 21:15). Following the removal of the background bins (Supp Table 2), reads were counted in cytobands in order to calculate the coverage for each cytoband. There were 1,293 cytobands downloaded from the UCSC genome browser. Unlocalized sequences were removed from the analysis leaving a total of 863 cytobands for subsequent analyses. For figures containing 1-kb HCBs in cytobands, the number of top 1,000 high coverage GAPF bins corresponding to each cytoband were counted.

Tumor Fraction:

DNA copy number (CN) and tumor fraction (TF) were computed from shallow whole genome sequencing data using the hidden Markov model implemented in the software package ichorCNA (v0.3.2).[65] (*read counter options: --window 1000000 --quality 20 --chromosome "chr1, chr2, chr3, chr4, chr5, chr6, chr7, chr8, chr9, chr10, chr11, chr12, chr13, chr14, chr15, chr16, chr17, chr18, chr19, chr20, chr21, chr22, chrX, chrY"*) (*runIchorCNA options: --ploidy "c(2,3)" --normal "c(0.5,0.6,0.7,0.8,0.9)" --maxCN 3 --gcWig gc_hg38_1000kb.wig --mapWig map_hg38_1000kb.wig --centromere GRCh38.GCA_000001405.2_centromere_acen.txt --normalPanel HD_ULP_PoN_hg38_1Mb_median_normAutosome_median.rds --includeHOMD False --chrs "c(1:22, \"X\")" --chrTrain "c(1:22)" --estimateNormal True --estimatePloidy True --estimateScPrevalence False --scStates "c()" --txnE 0.9999 --txnStrength 10000*)

GAPF Binary Classifier (Threshold Model):

The normalized read coverage in 1 kb non-overlapping bins following the mapping quality score filter (MAPQ score >= 40) were sorted in descending order (*sort options: -nr -k 4 -k 2n*). The top 1,000 bins according to coverage were considered for subsequent analyses (*head options: -1000*). The number of these high coverage bins (HCBs) corresponding to each chromosome were counted (totaling 1,000). A binary classifier designated samples as GAPF-positive or GAPF-negative according to the number of HCBs on a chromosome against a threshold. Using the 39 breast tumor and normal samples, the sensitivity and specificity were calculated at various thresholds for HCBs on a chromosome. A receiver operating characteristic curve (ROC) was generated and the area under the curve (AUC) was calculated using the trapezoidal rule. The optimal threshold was determined using Youden's J statistic.

Automated Machine Learning Pipeline (STREAMLINE):

Machine learning binary classification modeling and evaluation was conducted using version 0.2.5 of the Simple Transparent End-To-End Automated Machine Learning Pipeline (STREAMLINE),[47] applying mostly default pipeline run parameters (exceptions identified below). Input data were the number of top 1,000 HCBs on chromosomes 1-22 and X (23 features) unless otherwise stated. Three-fold cross-validation (CV) was used in the predictive modeling using the following classification algorithms: Naïve-Bayes (NB), Random Forest (RF), Extreme Gradient Boosting (XGB),[66] Category Gradient Boosting (CGB),[67] or Extended Supervised Tracking and Classifying System (ExSTraCS).[68] Within STREAMLINE, all algorithms with hyperparameters

(excluding NB) underwent an Optuna-driven hyperparameter sweep[69] with 200 target trials and a timeout of 15 minutes across a broad range of hyperparameter options. In addition to evaluating all models across 16 classification metrics, STREAMLINE also calculates model feature importance estimates uniformly for each algorithm and model using permutation feature importance estimation. STREAMLINE model training was repeated for each analysis using random seeds of 22, 32, or 42 unless otherwise stated.

References

1. Hanahan, D. Hallmarks of Cancer: New Dimensions. *Cancer Discovery* **12**, 31-46 (2022).
2. Alexandrov, L.B.*, et al.* The repertoire of mutational signatures in human cancer. *Nature* **578**, 94-101 (2020).
3. Li, Y.*, et al.* Patterns of somatic structural variation in human cancer genomes. *Nature* **578**, 112-121 (2020).
4. Aaltonen, L.A.*, et al.* Pan-cancer analysis of whole genomes. *Nature* **578**, 82-93 (2020).
5. Nik-Zainal, S.*, et al.* Landscape of somatic mutations in 560 breast cancer whole-genome sequences. *Nature* **534**, 47-54 (2016).
6. Ignatiadis, M., Sledge, G.W. & Jeffrey, S.S. Liquid biopsy enters the clinic — implementation issues and future challenges. *Nature Reviews Clinical Oncology* **18**, 297-312 (2021).
7. Schwarzenbach, H., Hoon, D.S.B. & Pantel, K. Cell-free nucleic acids as biomarkers in cancer patients. *Nature Reviews Cancer* **11**, 426-437 (2011).
8. Prensner, J.R., Rubin, M.A., Wei, J.T. & Chinnaiyan, A.M. Beyond PSA: the next generation of prostate cancer biomarkers. *Sci Transl Med* **4**, 127rv123 (2012).
9. Swisher, E.M.*, et al.* Rucaparib in relapsed, platinum-sensitive high-grade ovarian carcinoma (ARIEL2 Part 1): an international, multicentre, open-label, phase 2 trial. *Lancet Oncol* **18**, 75-87 (2017).
10. Gadgeel, S.M. LBA81_PR - P hase II/III blood-first assay screening trial (BFAST) in treatment-naïve NSCLC: initial results from the ALK+ cohort. *Annals of Oncology* **30**(2019).
11. André, F.*, et al.* Alpelisib for PIK3CA-Mutated, Hormone Receptor-Positive Advanced Breast Cancer. *N Engl J Med* **380**, 1929-1940 (2019).
12. André, F.*, et al.* Alpelisib plus fulvestrant for PIK3CA-mutated, hormone receptor-positive, human epidermal growth factor receptor-2-negative advanced breast cancer: final overall survival results from SOLAR-1. *Ann Oncol* **32**, 208-217 (2021).
13. Abida, W.*, et al.* Non-BRCA DNA Damage Repair Gene Alterations and Response to the PARP Inhibitor Rucaparib in Metastatic Castration-Resistant Prostate Cancer: Analysis From the Phase II TRITON2 Study. *Clin Cancer Res* **26**, 2487-2496 (2020).
14. Abida, W.*, et al.* Rucaparib in Men With Metastatic Castration-Resistant Prostate Cancer Harboring a BRCA1 or BRCA2 Gene Alteration. *J Clin Oncol* **38**, 3763-3772 (2020).
15. Hu, Y.*, et al.* False-Positive Plasma Genotyping Due to Clonal Hematopoiesis. *Clinical Cancer Research* **24**, 4437-4443 (2018).
16. Coombs, C.C.*, et al.* Identification of Clonal Hematopoiesis Mutations in Solid Tumor Patients Undergoing Unpaired Next-Generation Sequencing Assays. *Clin Cancer Res* **24**, 5918-5924 (2018).
17. Chabon, J.J.*, et al.* Integrating genomic features for non-invasive early lung cancer detection. *Nature* **580**, 245-251 (2020).
18. Meddeb, R., Pisareva, E. & Thierry, A.R. Guidelines for the Preanalytical Conditions for Analyzing Circulating Cell-Free DNA. *Clin Chem* **65**, 623-633 (2019).
19. Elazezy, M. & Joosse, S.A. Techniques of using circulating tumor DNA as a liquid biopsy component in cancer management. *Comput Struct Biotechnol J* **16**, 370-378 (2018).
20. Leary, R.J.*, et al.* Detection of Chromosomal Alterations in the Circulation of Cancer Patients with Whole-Genome Sequencing. *Science Translational Medicine* **4**, 162ra154-162ra154 (2012).

21. Leary, R.J., *et al.* Development of Personalized Tumor Biomarkers Using Massively Parallel Sequencing. *Science Translational Medicine* **2**, 20ra14-20ra14 (2010).
22. Mouliere, F., *et al.* Enhanced detection of circulating tumor DNA by fragment size analysis. *Science Translational Medicine* **10**, eaat4921 (2018).
23. Cristiano, S., *et al.* Genome-wide cell-free DNA fragmentation in patients with cancer. *Nature* **570**, 385-389 (2019).
24. Mathios, D., *et al.* Detection and characterization of lung cancer using cell-free DNA fragmentomes. *Nat Commun* **12**, 5060 (2021).
25. Vagner, T., *et al.* Large extracellular vesicles carry most of the tumour DNA circulating in prostate cancer patient plasma. *J Extracell Vesicles* **7**, 1505403 (2018).
26. Tanaka, H., Bergstrom, D.A., Yao, M.C. & Tapscott, S.J. Widespread and nonrandom distribution of DNA palindromes in cancer cells provides a structural platform for subsequent gene amplification. *Nat Genet* **37**, 320-327 (2005).
27. Guenthoer, J., *et al.* Assessment of palindromes as platforms for DNA amplification in breast cancer. *Genome Res* **22**, 232-245 (2012).
28. Marotta, M., *et al.* Homology-mediated end-capping as a primary step of sister chromatid fusion in the breakage-fusion-bridge cycles. *Nucleic Acids Res* **41**, 9732-9740 (2013).
29. Murata, M.M., Giuliano, A.E. & Tanaka, H. Genome-Wide Analysis of Palindrome Formation with Next-Generation Sequencing (GAPF-Seq) and a Bioinformatics Pipeline for Assessing De Novo Palindromes in Cancer Genomes. in *Cancer Systems and Integrative Biology* (eds. Kasid, U.N. & Clarke, R.) 13-22 (Springer US, New York, NY, 2023).
30. Yang, H., *et al.* GAP-Seq: a method for identification of DNA palindromes. *BMC Genomics* **15**, 394 (2014).
31. Campbell, P.J., *et al.* The patterns and dynamics of genomic instability in metastatic pancreatic cancer. *Nature* **467**, 1109-1113 (2010).
32. Skaletsky, H., *et al.* The male-specific region of the human Y chromosome is a mosaic of discrete sequence classes. *Nature* **423**, 825-837 (2003).
33. Warburton, P.E., Giordano, J., Cheung, F., Gelfand, Y. & Benson, G. Inverted repeat structure of the human genome: the X-chromosome contains a preponderance of large, highly homologous inverted repeats that contain testes genes. *Genome Res* **14**, 1861-1869 (2004).
34. Tanaka, H. & Watanabe, T. Mechanisms Underlying Recurrent Genomic Amplification in Human Cancers. *Trends Cancer* **6**, 462-477 (2020).
35. Lee, J.J.-K., *et al.* ERα-associated translocations underlie oncogene amplifications in breast cancer. *Nature* **618**, 1024-1032 (2023).
36. Kim, H., *et al.* Extrachromosomal DNA is associated with oncogene amplification and poor outcome across multiple cancers. *Nat Genet* **52**, 891-897 (2020).
37. Rudolph, K.L., Millard, M., Bosenberg, M.W. & DePinho, R.A. Telomere dysfunction and evolution of intestinal carcinoma in mice and humans. *Nature Genetics* **28**, 155-159 (2001).
38. Diede, S.J., *et al.* DNA methylation of developmental genes in pediatric medulloblastomas identified by denaturation analysis of methylation differences. *Proc Natl Acad Sci U S A* **107**, 234-239 (2010).
39. Marotta, M., *et al.* Palindromic amplification of the ERBB2 oncogene in primary HER2-positive breast tumors. *Sci Rep* **7**, 41921 (2017).
40. Wu, S., *et al.* Circular ecDNA promotes accessible chromatin and high oncogene expression. *Nature* **575**, 699-703 (2019).
41. Tanaka, H., Tapscott, S.J., Trask, B.J. & Yao, M.C. Short inverted repeats initiate gene amplification through the formation of a large DNA palindrome in mammalian cells. *Proc Natl Acad Sci U S A* **99**, 8772-8777 (2002).
42. Rattray, A.J., Shafer, B.K., Neelam, B. & Strathern, J.N. A mechanism of palindromic gene amplification in Saccharomyces cerevisiae. *Genes Dev* **19**, 1390-1399 (2005).
43. Nik-Zainal, S., *et al.* Landscape of somatic mutations in 560 breast cancer whole-genome sequences. *Nature* (2016).

44. Ganapathiraju, M.K., Subramanian, S., Chaparala, S. & Karunakaran, K.B. A reference catalog of DNA palindromes in the human genome and their variations in 1000 Genomes. *Human Genome Variation* **7**, 40 (2020).
45. Zou, X.*, et al.* Short inverted repeats contribute to localized mutability in human somatic cells. *Nucleic Acids Res* **45**, 11213-11221 (2017).
46. Maser, R.S. & DePinho, R.A. Connecting chromosomes, crisis, and cancer. *Science* **297**, 565-569 (2002).
47. Urbanowicz, R., Zhang, R., Cui, Y. & Suri, P. STREAMLINE: A Simple, Transparent, End-To-End Automated Machine Learning Pipeline Facilitating Data Analysis and Algorithm Comparison. in *Genetic Programming Theory and Practice XIX* (eds. Trujillo, L., Winkler, S.M., Silva, S. & Banzhaf, W.) 201-231 (Springer Nature Singapore, Singapore, 2023).
48. Tong, B.*, et al.* Comparing Amyloid Imaging Normalization Strategies for Alzheimer's Disease Classification using an Automated Machine Learning Pipeline. *AMIA Jt Summits Transl Sci Proc* **2023**, 525-533 (2023).
49. Hwang, S.*, et al.* Toward Predicting 30-Day Readmission Among Oncology Patients: Identifying Timely and Actionable Risk Factors. *JCO Clin Cancer Inform* **7**, e2200097 (2023).
50. Rengasamy, D.*, et al.* Feature importance in machine learning models: A fuzzy information fusion approach. *Neurocomputing* **511**, 163-174 (2022).
51. van der Pol, Y. & Mouliere, F. Toward the Early Detection of Cancer by Decoding the Epigenetic and Environmental Fingerprints of Cell-Free DNA. *Cancer Cell* **36**, 350-368 (2019).
52. Crawford, E.D.*, et al.* Androgen-targeted therapy in men with prostate cancer: evolving practice and future considerations. *Prostate Cancer and Prostatic Diseases* **22**, 24-38 (2019).
53. Sumiyoshi, T.*, et al.* Clinical utility of androgen receptor gene aberrations in circulating cell-free DNA as a biomarker for treatment of castration-resistant prostate cancer. *Scientific Reports* **9**, 4030 (2019).
54. van Dessel, L.F.*, et al.* The genomic landscape of metastatic castration-resistant prostate cancers reveals multiple distinct genotypes with potential clinical impact. *Nature Communications* **10**, 5251 (2019).
55. Wang, Y.K.*, et al.* Genomic consequences of aberrant DNA repair mechanisms stratify ovarian cancer histotypes. *Nat Genet* **49**, 856-865 (2017).
56. Coombes, R.C.*, et al.* Personalized Detection of Circulating Tumor DNA Antedates Breast Cancer Metastatic Recurrence. *Clin Cancer Res* **25**, 4255-4263 (2019).
57. Kotani, D.*, et al.* Molecular residual disease and efficacy of adjuvant chemotherapy in patients with colorectal cancer. *Nature Medicine* **29**, 127-134 (2023).
58. de Bono, J.S.*, et al.* Abiraterone and increased survival in metastatic prostate cancer. *N Engl J Med* **364**, 1995-2005 (2011).
59. Scher, H.I.*, et al.* Increased survival with enzalutamide in prostate cancer after chemotherapy. *N Engl J Med* **367**, 1187-1197 (2012).
60. Cui, X., Schiff, R., Arpino, G., Osborne, C.K. & Lee, A.V. Biology of Progesterone Receptor Loss in Breast Cancer and Its Implications for Endocrine Therapy. *Journal of Clinical Oncology* **23**, 7721-7735 (2005).
61. Aigner, M. Variants of the majority problem. *Discrete Applied Mathematics* **137**, 3-25 (2004).
62. Iqbal, M., Browne, W.N. & Zhang, M. Reusing Building Blocks of Extracted Knowledge to Solve Complex, Large-Scale Boolean Problems. *IEEE Transactions on Evolutionary Computation* **18**, 465-480 (2014).
63. Saarela, M. & Jauhiainen, S. Comparison of feature importance measures as explanations for classification models. *SN Applied Sciences* **3**, 272 (2021).
64. Klein, E.A.*, et al.* Clinical validation of a targeted methylation-based multi-cancer early detection test using an independent validation set. *Ann Oncol* **32**, 1167-1177 (2021).
65. Adalsteinsson, V.A.*, et al.* Scalable whole-exome sequencing of cell-free DNA reveals high concordance with metastatic tumors. *Nat Commun* **8**, 1324 (2017).

66. Chen, T. & Guestrin, C. XGBoost: A Scalable Tree Boosting System. in *Proceedings of the 22nd ACM SIGKDD International Conference on Knowledge Discovery and Data Mining* 785–794 (Association for Computing Machinery, San Francisco, California, USA, 2016).
67. Dorogush, A.V., Ershov, V. & Gulin, A. CatBoost: gradient boosting with categorical features support. *ArXiv* **abs/1810.11363**(2018).
68. Urbanowicz, R.J. & Moore, J.H. ExSTraCS 2.0: Description and Evaluation of a Scalable Learning Classifier System. *Evol Intell* **8**, 89-116 (2015).
69. Akiba, T., Sano, S., Yanase, T., Ohta, T. & Koyama, M. Optuna: A Next-generation Hyperparameter Optimization Framework. in *Proceedings of the 25th ACM SIGKDD International Conference on Knowledge Discovery & Data Mining* 2623–2631 (Association for Computing Machinery, Anchorage, AK, USA, 2019).

Acknowledgement

This work is supported by the National Cancer Institute (2 R01 CA149385), Department of Defense (W81XWH-18-1-0058), and Cedars-Sinai Medical Center (to H.T.); the Margie and Robert E. Petersen Foundation (to A.E.G.).

Author Contributions

M.M.M., A.E.G. and H.T. conceived and designed the experiments. M.M.M., F.I. and L.M. generated genomic data. M.M.M., F.I. and H.T. designed the data analysis workflow. M.M.M. and S.K. performed statistical analyses. R.U. designed the ML pipeline software, interpreted the analyses, and revised the manuscript. Z.C. and E.M.P. provided prostate cancer samples and interpreted the data. M.M.M. and H.T. wrote the manuscript. D.D., A.E.G. and H.T. supervised the project.

Competing interests

The authors declare no competing interests.